J Exp Biol Advance Online Articles. First posted online on 29 July 2016 as doi:10.1242/jeb.136721
Access the most recent version at http://jeb.biologists.org/lookup/doi/10.1242/jeb.136721

Aerodynamic consequences of wing morphing during emulated take-off and gliding in birds

KEYWORDS: advance ratio, wing, flapping, gliding, morphing, propeller

Brett Klaassen van Oorschot[1*]; Emily A. Mistick[2]; Bret W. Tobalske[1]

[1]Field Research Station at Fort Missoula, Division of Biological Sciences, University of
Montana, Missoula, MT 59812, USA.

[2]Concord Field Station, Department of Organismic and Evolutionary Biology, Harvard University, Cambridge, MA 02138

*Author for correspondence
Email: brett.kvo@umontana.edu

SUMMARY STATEMENT

We measured swept and extended bird wings during emulated flapping and gliding to discover how morphing wing posture affects performance.

ABSTRACT

Birds morph their wings during a single wingbeat, across flight speeds, and among flight modes. Such morphing may allow them to maximize aerodynamic performance, but this assumption remains largely untested. We tested the aerodynamic performance of swept and extended wing postures of 13 raptor species in three families (Accipitridae, Falconidae, and Strigidae) using a propeller model to emulate mid-downstroke of flapping during takeoff and a wind tunnel to emulate gliding. Based on previous research, we hypothesized that 1) during flapping, wing posture would not affect maximum ratios of vertical and horizontal force coefficients (C_V:C_H), and that 2) extended wings would have higher maximum C_V:C_H when gliding. Contrary to each hypothesis, during flapping, extended wings had, on average, 31% higher max C_V:C_H ratios and 23% higher C_V than swept wings across all biologically relevant attack angles (α), and, during gliding, max C_V:C_H ratios were similar for both postures. Swept wings had 11% higher C_V than extended wings in gliding flight, suggesting flow conditions around these flexed raptor wings may be different from those in previous studies of swifts (Apodidae). Phylogenetic affiliation was a poor predictor of wing performance, due in part to high intrafamilial variation. Mass was only significantly correlated with extended wing performance during gliding. We conclude wing shape has a greater effect on force per unit wing area during flapping at low advance ratio, such as take-off, than during gliding.

Journal of Experimental Biology • Advance article

INTRODUCTION

Flying birds use their wings to accomplish a diverse range of behaviors, including takeoff and landing, maneuvering, cruising, and soaring flight. Aerodynamic performance during each type of locomotion may be maximized by altering wing configuration, and birds often dynamically readjust their wing posture as they transition from one behavior to another or as they interact with varying aerodynamic conditions. In particular, birds partially retract their wings into a swept configuration during a variety of aerial behaviors. For example, birds sweep back their wings during upstroke in response to changing flight speeds and modulate wing flexion according to speed and glide angle (Pennycuick, 1968; Tucker, 1987; Tucker and Parrott, 1970). Swifts actively modify wing sweep to alter sink speed and turning rate during maneuvers (Lentink et al., 2007). Eagles sweep their wings back in response to turbulence (Reynolds et al., 2014). Dynamic (i.e. instantaneously variable) wing morphing appears to be ubiquitous among flying birds, and it is generally hypothesized that such morphing optimizes aerodynamic performance.

Although wing morphing is known to alter flight performance during high-speed gliding in ways that influence maneuvering (Lentink et al., 2007), the aerodynamic consequences of wing morphing at different flight speeds and between flapping and gliding is not well-understood. As birds transition from slow to high speed, they continue to flap their wings. During this transition, the body velocity relative to wingtip velocity increases. This relationship is called advance ratio (J):

$$J = \frac{V}{\Omega b} \quad \text{(Eq. 1)}$$

where V = free-stream velocity (m s^{-1}), Ω = angular velocity of the wing (rad s^{-1}), and b = wing length (m). During hovering and very slow flight, such as immediately after takeoff or

before landing, *J* is zero and very low, respectively (Provini et al., 2012; Provini et al., 2014; Tobalske, 2007). *J* increases with increasing translational velocity of the whole bird, going to infinity during gliding. We tested the effects of swept and extended wing configurations on aerodynamic performance at low and high *J*.

Current understanding suggests that during flapping flight, subtleties of wing shape have little impact on aerodynamic performance (Usherwood and Ellington, 2002a; Usherwood and Ellington, 2002b). Specifically, propeller models that emulate the mid-downstroke of flapping flight at low-*J* reveal that aspect ratio (*AR*, wing span/average wing chord) has virtually no effect on aerodynamic force coefficients except at the highest angles of attack (α) that are probably not biologically relevant for birds (Usherwood and Ellington, 2002a; Usherwood and Ellington, 2002b). For gliding ($J=\infty$), it has long-been assumed that selective pressures have promoted aerodynamic efficiency (i.e. lift:drag ratio) among flying animals (Allen, 1888; Averill, 1927; Beaufrère, 2009; Savile, 1957). The most efficient gliding birds are presumed to be those with either long, high-aspect ratio wings (e.g. frigatebirds and albatrosses) or emarginated, vertically separated primary feathers (e.g. hawks and vultures). These morphologies exhibit extended wings and increase span efficiency by minimizing induced drag caused by the wing-tip vortex (Henningsson et al., 2014; Spedding and McArthur, 2010). In both cases, these efficient wings minimize the effect of the wing-tip vortex by either 1) increasing aspect ratio and thereby reducing the strength of the wingtip vortex(Viieru et al., 2006), or 2) dispersing and shedding the wing-tip vortex away from the upper surface of the wing in a manner similar to winglets on aircraft (Tucker, 1993; Tucker, 1995).

Cumulatively, these studies led us to form two hypotheses: First, we hypothesized that at low-*J*, both swept and extended wings should produce similar aerodynamic force coefficients (H_1). Second, we hypothesized that at high-*J*, extended wings (due to their

increased span and slotted distal primary feathers) should have higher ratios of vertical to horizontal force coefficients (C_V:C_H) compared with swept wings (H_2).

To test these hypotheses, we studied wing performance in 13 raptor species (falcons, hawks, and owls; Falconidae, Accipitridae, and Strigidae) using a propeller model (see Usherwood, 2009; Heers et al., 2011), emulating wing translation during mid-downstroke at low-*J* as in takeoff or landing, and in a wind tunnel, emulating gliding when $J=\infty$. The species in our sample had varying degrees of slotted distal wing planforms when their wings were extended due to emargination of their primary feathers. These birds routinely engage in take-off and landing (low-*J*) and intermittent flight consisting of flapping phases interspersed with glides *(*high-*J)*. At low-*J*, birds always flap their wings fully extended. Our study, however, allowed us to explore the aerodynamics associated with swept wings at low-*J*, which could be useful in understanding why birds take off with fully extended wings and also in aiding the design of bird-like micro air vehicles (MAVs). Furthermore, the natural variation in wing shape across the 13 species in this study allowed us to test for aerodynamic differences among clades and explore the evolutionary context of wing morphing.

MATERIALS AND METHODS

Specimens

We measured 26 wings from 13 species of raptors, a large, multiphyletic guild. These birds ranged in mass from 81 g to 1860 g (Table 1). We gathered specimens that had already died from a variety of causes unrelated to this study, and many were missing organs or had become severely dehydrated. For this reason, some masses were estimated using averaged sex-specific values (Dunning Jr., 1992) and are denoted with an asterisk (*) in Table 1.

Wing Preparation

We removed the wings from the bird at the shoulder between the humeral head and the glenoid cavity. We then positioned them in either an extended or swept configuration (Fig. 1), pinned them on a foam board, and dried them at 50° C for 1-3 weeks until the connective tissue hardened. Extended angles were chosen based on the maximum the skeleton and connective tissues would allow, generally forming a straight leading edge. Swept angles were approximated at ~40°, but often changed during drying as the connective tissue contracted. Post-hoc sweep angles were measured between the humeral head, wrist joint, and tip of the leading-edge primary feather, and are reported in Table 1. Once the wings had dried, we drilled into the head of the exposed humerus and inserted a brass tube (4-5 mm dia.) into the hollow bone matrix, cementing it in place using Devcon 5 Minute® epoxy. The brass tubes were counterbalanced internally so we could avoid oscillations associated with spinning unbalanced wings.

Morphometrics, attack angle, and analysis

We measured wing characteristics by photographing and then analyzing them in ImageJ (Schneider et al., 2012). We computed moments of area using a custom MATLAB script (The Mathworks Inc.) (see Table S1). We determined feather emargination based on a

prior measure of whole-wing porosity (Heers et al., 2011):

$$Feather\ Emargination = 100\ \left(\frac{potential\ wing\ area}{actual\ wing\ area}\right) - 100$$

(Eq. 2)

We used a lateral view of the distal 1/3 of the wing to set geometric angle of attack (α) prior to aerodynamically loading the wings, but considered the attack angle to be zero when lift was zero. Spanwise twist (i.e. washout) was a ubiquitous characteristic among the wings, and the wings deformed under aerodynamic load (Heers et al., 2011) causing the local α to vary greatly. To obtain an objective measure of zero-lift α for comparison among wings, we first interpolated our force values at 1° increments using a cubic spline between empirical measurements for α ranging from -5°<α<+50°. Then we adjusted our measured α to be zero when lift was 0 N.

When possible, we report differences between swept and extended wings using the following percent-change formula, where relevant values (e.g. C_V or F_V) are substituted:

$$Percent\ Change = \frac{(extended\ wing - swept\ wing)}{(extended\ wing)} \times 100$$

(Eq. 3)

Wind tunnel measurements

To explore the aerodynamics associated with high-*J*, translational flight, we used custom wind tunnels at the Flight Laboratory at the University of Montana (Tobalske et al., 2005) and the Concord Field Station at Harvard University (Tobalske et al., 2003a). We

sampled each wing at 8 ms^{-1}. The wing was affixed with a brass rod to a NEMA 23 stepper motor (23W108D-LW8, Anaheim Automation, Inc.) fastened to a force plate (see *Force Measurements* below for details), located outside the tunnels. The wings were rotated through attack angles in 4.5° increments, controlled using an Arcus ACE-SDE controller (Arcus Technology Inc., Livermore, CA, USA). We calculated Reynolds number (*Re*) by measuring the wing chord at the base of the alula feather. To test for effects of aeroelastic deformation at higher velocities, we tested a subset of the wings at 10 ms^{-1} and 14.1ms^{-1} and noted no difference in the vertical or horizontal coefficients. Those results are omitted here for simplicity.

Propeller measurements

We spun the wings like a propeller to emulate mid-downstroke during low-*J* flapping flight (Heers et al., 2011; Usherwood, 2009; Usherwood and Ellington, 2002a; Usherwood and Ellington, 2002b). We applied estimated *in vivo* angular velocities (rad s^{-1}) using known wing-beat frequencies and stroke excursion angles from prior studies (Jackson and Dial, 2011; Tobalske and Dial, 2000). For birds <800g in body mass, we used $\log \Omega = .01966(\log(m)) + 2.0391$ and for birds >800 g, we used $\log \Omega = .3055(\log(m)) + 2.1811$, where Ω is angular velocity and m is mass. The larger birds' wings broke when spun using the angular velocity equation of the smaller birds, necessitating the second equation fitted specifically to birds >800 g. We measured the vertical force and torque these wings generated using 5°-10° increments in α. We ran several of the wings at various angular velocities and noted no significant difference in the resulting coefficients of aerodynamic force.

For <800 g birds, we used a NEMA 23 stepper motor (23W108D-LW8, Anaheim Automation, Inc.). For >800 g birds, we used NEMA 34 stepper motor (34Y314S-LW8,

Anaheim Automation, Inc.) coupled with a 3:1 planetary inline reduction gearbox (GBPH-060x-NP, Anaheim Automation, Inc.). Both motors were controlled using the same Arcus controller used in the wind tunnel measurements.

Force Measurements

We measured aerodynamic forces using a custom force plate (15×15cm platform, 200Hz resonant frequency, Bertec Corporation, Columbus, OH, USA) for wings from birds <800 g, and a Kistler type-9286A force plate (Kistler Instruments Corp., Amherst, NY, USA) for wings from birds >800 g. At each α, we collected data at 1 KHz for several seconds and then filtered those force traces using a 3-Hz low-pass Butterworth filter before taking an average of the forces over the duration of the measurement. Raw force traces contained considerable noise due to aeroelastic flutter (Fig. 2).

For comparisons among wings, we nondimensionalized the forces into vertical and horizontal coefficients using the following equations (see Usherwood and Ellington, 2002a):

Flapping flight:

$$C_V = \frac{2F_V}{\rho\Omega^2 S_2} \qquad C_H = \frac{2Q}{\rho\Omega^2 S_3}$$

(Eq. 4)

Gliding flight:

$$C_V = \frac{2F_V}{\rho V^2 S} \qquad C_H = \frac{2F_H}{\rho V^2 S}$$

(Eq. 5)

where C_V is the coefficient of vertical force, C_H is the coefficient of horizontal force, F_V is vertical force (N), F_H is the horizontal force (N), Q is torque (N m) about the z-axis, ρ is air density at Missoula, MT, (978 m elev., 1.07 kg/m^3), or Bedford, MA (41 m elev., 1.204 kg/m^3), Ω is angular velocity of the spinning wing (rad s^{-1}), S is the area (m^2), S_2 is the

second moment of area of the wing (m^4), and S_3 is the third moment of area of the wing (m^5, Table S1).

Statistics and phylogenetic analysis

To test for effects of mass on peak C_V:C_H values, we used phylogenetically independent contrasts (PIC; see Felsenstein, 1985) computed using a consensus tree of our experimental species downloaded from birdtree.org (Jetz et al., 2012; Revell, 2012). We tested for effects at the family-level using phylogenetic ANOVAs (R Core Team, 2015; Revell, 2012). We compared continuous variables using phylogenetically independent contrasts within linear models. We used paired T-tests to test for significant differences between swept and extended wings in peak force coefficients and absolute force. We report means ± 1 SD.

RESULTS

Flapping coefficients

For the propeller model (emulating mid-downstroke of flapping at J=0), extended wings had significantly higher peak C_V:C_H than swept wings ($p<.0001$, paired T-test) (Fig. 3). On average, peak C_V:C_H was 3.7±0.8 for extended wings and 2.6±0.9 for swept wings, a 30.9% difference. Changes in C_V were responsible for most differences in C_V:C_H between swept and extended wings (Fig. 4, 5). Swept-wing average peak C_V was 23.1±32.3% lower than extended wings, and average peak C_H was 2.0±59.4% lower. Differences between average swept and extended peak C_V were statistically significant ($p<0.004$) and differences in average peak C_H were nearly significant ($p=0.08$).

The angles at which average peak C_V:C_H occurred were α=17.5°±2.8° for extended wings and α=22.3°±9.2° for swept wings. The highest individual C_V:C_H recorded was 4.8 at α=18° for the extended flapping wing of the rough-legged hawk (*Buteo lagopus*). The red-tailed hawk (*Buteo jamaicensis*) had the highest swept C_V, 1.2, at α=44°, while the rough-legged hawk (*Buteo lagopus*) exhibited the highest extended C_V, 2.0, at α=43° (Table 3, Fig. 6, Table S2).

Gliding coefficients

During modeled gliding flight in the wind tunnel (where $J=\infty$), peak swept and extended wing C_V:C_H ratios were not significantly different (p=0.5, paired T-test; Fig. 3 & 4). The average for extended wings was 4.8±1.1 at α=13.1°±2.1°, while the average peak C_V:C_H ratio for swept wings was 4.7±1.6 at α=12.6°±1.9°, a difference of only 0.7%. Similar to flapping, C_V mediated most of the differences in C_V:C_H. In gliding, the swept wings average peak C_V was 10.6±23.5% higher than extended wings, while average peak C_H was 2.8±14.8% lower (Fig. 4, 5).

The swept wing of the great horned owl (*Bubo virgianus*) had the highest individual peak C_V:C_H, 7.9, at α=11°. The peregrine falcon (*Falco peregrinus*) had the highest swept C_V, 1.4, at α=38°, while the great-horned owl exhibited the highest extended C_V, 1.4, at α=40° (Table 3, Fig. 6, Table S2).

Absolute forces

Absolute forces varied greatly due to differences in wing area (S), shape, and, in the propeller model, angular velocity (Ω), second moment of area (S_2), and third moment of area (S_3). Swept wings had 26.6±10.3% less area, 57.9±14.4% lower S2, and 68.2±14.1% lower S3 than extended wings (Table S1).

During emulated flapping, swept wings produced 68.0±16.1% less peak F_V and 68.9±22.0% less peak F_H than extended wings. The percent change between extended and swept wings for both peak F_V and F_H was not significantly different than the percent change in S_2 or S_3 ($p>0.1$, paired t-test, for both). During emulated gliding, swept wings produced on average 20.6±12.8% less peak vertical force (F_V) and 29.4±11.8% less peak horizontal force (F_H) than extended wings.

The extended wing of the great-horned owl produced the highest vertical force of all the wings tested during emulated gliding flight, 6.7 N (36.7% body weight per wing), at $\alpha=39°$ and $8 ms^{-1}$. The extended wing of this species produced 3.9 N (21.2% body weight per wing) during emulated flapping flight at $\alpha=44°$ and 15.2 $rads^{-1}$. During emulated flapping flight, the extended wing of the rough-legged hawk produced the highest vertical force, 4.4 N (54.0% body weight), at $\alpha=43°$ and 19.6 $rads^{-1}$. The American kestrel (*Falco sparverius*) wing produced the highest force as a percentage of body weight during modeled gliding flight at 66% (132% when considering two wings). The highest force relative to body weight observed on the propeller model came from the wing of the merlin (*Falco columbarius*). It supported 86.8% of body weight (167% for two wings.) On average, individual extended wings produced 47% weight support during emulated gliding flight and 48% weight support during emulated flapping flight. In emulated gliding flight, the average critical attack angle was $\alpha=32°\pm6°$ for swept wings and $\alpha=28°\pm6°$ for extended wings, while in emulated flapping flight, the average critical attack angle was $\alpha=48°\pm2°$ for swept wings and $\alpha=45°\pm4°$ for extended wings.

Interspecific and morphological patterns

During emulated gliding, accipiter wings had the highest average peak C_V:C_H ratios in both swept and extended configurations (5.3±1.2 and 5.5±0.7, respectively). Conversely, falcons had the lowest average peak C_V:C_H ratios in swept and extended wing configurations during emulated gliding (3.3±0.4 and 3.8±0.8, respectively). Owl wings had average peak C_V:C_H ratios during emulated gliding of 4.9±2.0 for swept wings and 4.4±1.0 for extended wings. During emulated flapping, swept and extended accipiter wings similarly had the highest average peak C_V:C_H ratios (2.9±0.4 and 4.2±0.7, respectively). Falcon (1.8±0.6 and 3.4±0.4, swept and extended) and owl (2.6±1.2 and 3.2±0.7, swept and extended) wings had lower average peak C_V:C_H ratios during emulated flapping. Despite this variation, peak C_V:C_H between families was not significant for any wing posture or flight style (phylogenetic ANOVA, $p>0.4$ for all).

Familial classification was a poor predictor of wing morphological characteristics. Body mass, extended-wing aspect ratio, emargination, area, and wing loading did not vary significantly among families ($p>0.6$ for all, phylogenetic ANOVA). Log-transformed mass, however, was significantly positively correlated with extended average gliding peak Cv:C_H ($p=.02$, $R^2=0.35$, PIC-linear model, Table 2) and nearly significantly positively correlated with swept gliding peak Cv:C_H ($p=.06$, $R^2=0.21$, PIC-linear model). Mass was not positively correlated with swept flapping or extended flapping peak Cv:C_H ($p=0.1$ and .2, $R^2=0.12$ and .07, respectively). Log-transformed extended-wing area was also positively correlated with extended gliding and swept flapping average peak Cv:C_H ($p=0.005$ and 0.036, $R^2=0.49$ and .28, respectively) and also marginally significantly correlated with swept gliding($p=0.061$) and extended flapping ($p=0.07$). No other morphological characteristics significantly

correlated with peak C_V:C_H (Table 2). Additionally, mass did not correlate with primary feather emargination (p=0.3, phylogenetic ANOVA). Familial means generally exhibited large standard deviations indicating substantial morphological variance among closely-related species.

DISCUSSION

Wing sweep differentially influenced aerodynamic performance on a per-unit-area-basis (i.e. C_V and C_H). During emulated flapping, extended wings outperformed swept wings in both C_V and C_V:C_H; whereas during emulated gliding, swept wings outperformed extended wings in C_V and matched performance in C_V:C_H. These results provide insight into the relationship between wing posture and aerodynamic performance in raptors.

In emulated flapping flight, angular velocity of the rotating wing causes the wing tips to move more quickly than the wing roots. Since aerodynamic forces vary with the square of local velocity, longer wings produce exponentially greater forces. Furthermore, local flow conditions (as indicated in the coefficients) likely change according to wing posture, and may influence aerodynamic forces. In flapping flight, extended wings had 23.1% higher C_V than swept wings. Thus, in flapping, the 68% increase in peak F_V from swept to extended posture is likely driven by the additive positive effects of S_2 (58% increase) and C_V as wings extend. Extended wings outperform swept wings, even after accounting for S_2, in flapping flight.

During low-*J* flapping flight, the performance of extended wings may benefit from emarginated primary feathers. Previous research has suggested emargination reduces induced drag and increases span efficiency in gliding flight (Spedding and McArthur, 2010; Tucker, 1993; Tucker, 1995). However, our broader comparative sample contrasts with

Tucker's findings, because we observed that the effects of tip emargination are likely significant during takeoff (low *J*) but not during gliding (high *J*). This finding may help to explain variation in wing-tip morphology among the diverse array of soaring birds. Raptors must regularly takeoff vertically from the ground and may thus have slotted feathers to increase C_V at low *J*. In contrast, pelagic soarers such as albatross (with pointed wing tips) may rarely experience low-*J* flight due to constant marine surface winds and long, nearly horizontal takeoff trajectories into a prevailing headwind, and indeed avoid flapping flight altogether during windless conditions (Shaffer et al., 2001; Weimerskirch et al., 2000). This could explain the remarkable variation in wing shape between terrestrial and pelagic soaring birds. Future work could explore this hypothesis.

During emulated gliding flight (high-*J*), swept wings had 10.6% higher peak C_V and similar peak C_V:C_H ratios to extended wings. These swept wings had higher vertical force coefficients than extended wings, but due to reduction in S, produced 21% less vertical aerodynamic force. Peak F_V in gliding is thus primarily influenced by the competing effects of reduced S and increased C_V exhibited by swept wings.

In the present study, swept wings during gliding appear to behave like the delta wings of aircraft. Previous work has shown that delta wings can produce lift at post-stall attack angles using vortex lift (Er-El and Yitzhak, 1988; Polhamus, 1966). Vortex lift is caused by flow separation at the leading edge of the wing, and is therefore commonly referred to as a "leading-edge vortex" (LEV). This flow forms a distinct vortex on the top of the wing which runs parallel to the leading edge, increasing lift in a nonlinear fashion. In our experiment, the average critical attack angle (peak C_V) during gliding was $\alpha=32°$ for swept wings and $\alpha=28°$ for extended wings. During flapping, however, both swept and extended wings had high average critical attack angles of $\alpha=48°$ and $\alpha=45°$, respectively. Future research could explore

this hypothesis to better understand the aerodynamic mechanism behind increased swept-wing C_V during gliding flight.

Overall, our results were contrary to our two initial hypotheses and surprising for both extremes of advance ratio (*J*). Usherwood and Ellington (2002b) show that the aerodynamics of small- and medium-sized revolving wings (*J*=0; Reynolds numbers [*Re*] = 1100 to 26000) are relatively insensitive to variations in wing morphology and aspect ratio (*AR*). This is the primary evidence that led us to develop our hypothesis (H1). However, close examination of their data indicates our results our consistent for revolving wings at moderate angles of attack ($10°<\alpha<30°$) given that extended wings exhibited higher *AR* than swept wings (Table 1). For example, at $\alpha=20°$, their model hawkmoth wing with *AR*=15.8 generated 43% higher C_V than their model quail wing with *AR*=4.53, while C_H was generally similar for each wing. This implies that the C_V:C_H ratio was also greater for the wing of higher *AR* (Usherwood and Ellington, 2002b, see their Fig. 4C and D) . Their results show that wings with $4.5<AR<15.8$ produce indistinguishable maximum C_V between $40°<\alpha<60°$, whereas the extended raptor wings in our study continued to exhibit higher C_V and C_V:C_H ratios up to $\alpha=50°$ (Figs. 3 & 4). Also, over the relevant range of attack angles, we observed a relatively greater effect for a given *AR* compared to Usherwood and Ellington (2002b). The range of *AR* tested by Usherwood and Ellington (2002b) varied by 3.5x whereas *AR* in our study varied by 1.4x. We thus conclude that extended wings outperform swept wings in emulated flapping flight when *J*=0, but future efforts should seek to test the relative contribution of feather emargination versus *AR*.

The more dramatic differences we report between wing conditions compared with the effects of *AR* upon performance in Usherwood and Ellington (2002b) may be due to a variety of other explanatory variables. Wings in our sample experienced $370,000<Re<1,290,000$, which is above the critical *Re* of 200,000 where the boundary layer flow transitions from

laminar to turbulent (Vogel, 1996). In contrast, Usherwood and Ellington (2002b) tested wings far smaller than those in our experiment, with a maximum *Re* of 26,000. This change in flow regime likely affects force production. In addition to changing *AR* as birds sweep back their wings, camber (cross-sectional profile), washout (spanwise twist), leading-edge angle, and the magnitude of primary feather emargination changes (Tucker, 1987; Withers, 1981). Heers and colleagues (2011) showed that wing porosity (herein called feather emargination) was associated with low lift coefficients and low lift:drag ratios. In our present study, extended wings exhibited greater feather emargination with less feather overlap than swept wings (Table 1). These changes in morphology could affect local flow conditions and increase span efficiency (Henningsson et al., 2014; Spedding and McArthur, 2010; Tucker, 1987; Tucker, 1993; Tucker, 1995). At low α, average swept wing C_H values were nearly double the extended wing values, further highlighting the potential benefits of emargination at low *J*.

Previous studies of gliding wings ($J=\infty$) show that changes in aspect ratio (*AR*) and sweep can influence aerodynamic forces (Lentink et al., 2007; Pennycuick, 1968; Tucker and Parrott, 1970). Lentink and colleagues (2007) in a study of swift wings (Apodidae) in which feathers do not exhibit significant emargination showed that the lift coefficient was reduced as wings became increasingly swept during gliding. Our results show the opposite trend in raptors. The wings in our sample varied from $1.7<AR<5.0$ and exhibited changes in sweep between 34° and 81° (Table 1), and, although not a statistically significant difference, swept wings had 10.6% higher C_V when $J=\infty$. Additionally, our results indicate almost no difference in peak C_V:C_H between swept and extended wings during emulated gliding flight. A hypothesis for future comparative study is that these differences among species are due to feather emargination.

While coefficients provide insight into the relative levels of force production across species and wing shapes that differ in size, absolute forces, rather than coefficients, are of greater immediate relevance to a bird. Flying at low *J* requires far greater power output than steady translational flight at moderate speeds (Rayner, 1999; Tobalske, 2007; Tobalske et al., 2003b). Slow flight is key to safe transitions between the air and terrestrial perches (Provini et al., 2012; Provini et al., 2014), some forms of prey capture (e.g. hawking, (Fitzpatrick, 1980; Tobalske, 1996), predator escape (Devereux et al., 2006; van den Hout et al., 2010), and sexually-selected displays. Thus, during these behaviors, birds are likely concerned about maximal force production, rather than efficiency (i.e. C_V:C_H).

Birds generally fully extend their wings during mid-downstroke, and most sweep their wings back during upstroke (Rayner, 1988; Tobalske, 2007). In free-flying thrush nightingales (*Luscinia luscinia*), the upstroke has been shown to become more aerodynamically active as flight speed increases (Spedding et al., 2003) and many species exhibit wing-tip reversal or hand-wing supination in which lift can be produced at very low *J* (Brown, 1963; Crandell and Tobalske, 2011; Crandell and Tobalske, 2015; Tobalske and Dial, 1996), but it is generally thought of as "recovery stroke" between successive downstrokes. It is hypothesized that birds may therefore be sweeping back their wings to reduce drag during the upstroke (Rayner, 1988; Tobalske, 2001). Our results provide additional indirect support for this hypothesis, as swept wings reduced horizontal (i.e. drag) forces 69% during flapping compared to extended wings.

For gliding, our results indicate there is a broad envelope of aerodynamic efficiency available (i.e. C_V:C_H). Since C_V:C_H changes very little as birds sweep their wings, gliding birds are likely able to modulate S without affecting their glide angle by increasing speed during swept-wing flight. This may allow them flexibility when choosing flight speeds to meet environmental demands, such as when gliding between or within thermals. In the

present study, wing sweep reduced area 26.6±10.3% on average. Since S and aerodynamic forces scale linearly, it is surprising that F_V does not decrease accordingly with S. As S decreases, F_V decreases by 20.9%. The increase in C_V that occurs with increasing wing sweep during gliding may provide raptors with a subtle mechanism to alter the *magnitude* of total absolute aerodynamic forces, while modulating angle of attack changes the *relationship* between vertical and horizontal forces.

It is important to note that living birds constantly morph their wings in ways that remain difficult to measure and understanding the precise mechanisms responsible for changes in aerodynamic performance remains challenging. Our propeller and wind tunnel models do not fully represent the complexity of what actually occurs during flapping and gliding flight (Bilo, 1971; Tobalske, 2007).

Conclusions

This experiment shows that wing sweep does not significantly influence C_V:C_H during modeled gliding flight (high *J)* but does have a significant effect on modeled flapping flight such as take-off and landing (low *J)*. Additionally, C_V is higher in swept wings than extended wings during gliding flight, which leads us to speculate that local flow conditions are affected by wing shape. The poor performance of swept wings during spinning offers an explanation for the seemingly universal use of a fully-extended wing posture during downstroke in flapping flight in birds (Tobalske and Dial, 1996; Tobalske et al., 2003a). We hypothesize that relatively low C_V and high C_H values observed for flexed wings during spinning was the result of unfavorable patterns of flow, for example, preventing the formation of a leading-edge vortex (Birch et al., 2004; Ellington et al., 1996; Wang et al., 2004) at low α, and

perhaps causing separation of flow (stall) at higher α. In contrast, flexed wings performed better in terms of F_V per unit area in gliding, questioning previous hypotheses regarding the functional significance of emarginated primaries as adaptations for efficiency during high-*J* flight. Future flow-visualization studies would be useful in testing these ideas.

ACKNOWLEDGEMENTS

We thank Andrew Biewener for use of the wind tunnel and force plate at the Concord Field Station, and Natalie Wright, Ondi Crino, Brandon Jackson, and Pat Little for their help and advice. Two anonymous reviewers provided insightful suggestions that helped us revise the manuscript. Finally, we thank Steven Vogel, who was an extraordinary mentor, a limitless source of brilliant ideas and wit, and remains an inspiration in our hearts and minds.

COMPETING INTERESTS

The authors have no competing interests.

FUNDING

This research was supported by National Science Foundation grants GRFP DGE−1313190 to BKVO and IOS-0923606, IOS-0919799 and CMMI 1234747 to BWT. Undergraduate research support to EAM was provided by the Herchel-Smith Harvard Research Award.

LIST OF SYMBOLS

J = advance ratio

AR = aspect ratio

α = angle of attack

V = free-stream velocity (m s^{-1}),

Ω = angular velocity of the wing (rad s^{-1})

b = wing length (m).

C_V = coefficient of vertical force

C_H = coefficient of horizontal force

Re = Reynolds number

F_V = vertical force (N)

F_H = horizontal force (N)

Q = torque (N•m) about the z-axis,

ρ = air density

S = wing area (m^2),

S_2 = second moment of area of the wing (m^4)

S_3 = third moment of area of the wing (m^5).

REFERENCES

Allen, J. A. (1888). On the structure of birds in relation to flight, with special reference to recent alleged discoveries in the mechanism of the wing. *Trans. New York Acad. Sci.* 89–100.

Averill, C. K. (1927). Emargination of the long primaries in relation to power of flight and migration. *Condor* **29**, 17–18.

Beaufrère, H. (2009). A review of biomechanic and aerodynamic considerations of the avian thoracic limb. *J. Avian Med. Surg.* **23**, 173–185.

Bilo, D. (1971). Flugbiophysik von Kleinvögeln. *J. Comp. Physiol. A Neuroethol. Sensory, Neural, Behav. Physiol.* **71**, 382–454.

Birch, J. M., Dickson, W. B. and Dickinson, M. H. (2004). Force production and flow structure of the leading edge vortex on flapping wings at high and low Reynolds numbers. *J. Exp. Biol.* **207**, 1063–1072.

Brown, R. H. J. (1963). The flight of birds. *Biol. Rev.* **38**, 460–489.

Crandell, K. E. and Tobalske, B. W. (2011). Aerodynamics of tip-reversal upstroke in a revolving pigeon wing. *J. Exp. Biol.* **214**, 1867–1873.

Crandell, K. E. and Tobalske, B. W. (2015). Kinematics and aerodynamics of avian upstrokes during slow flight. *J. Exp. Biol.* **218**, 2518–27.

Devereux, C. L., Whittingham, M. J., Fernández-Juricic, E., Vickery, J. A. and Krebs, J. R. (2006). Predator detection and avoidance by starlings under differing scenarios of predation risk. *Behav. Ecol.* **17**, 303–309.

Dunning Jr., J. B. (1992). *CRC Handbook of avian body masses*. CRC Press.

Ellington, C. P., van den Berg, C., Willmott, A. P. and Thomas, A. L. R. (1996). Leading-edge vortices in insect flight. *Nature* **384**, 626–630.

Er-El, J. and Yitzhak, Z. (1988). Influence of the aspect ratio on the aerodynamics of the delta wing at high angle of attack. *J. Aircr.* **Vol. 25**, pp. 200–205.

Felsenstein, J. (1985). Phylogenies and the Comparative Method. *Am. Nat.* **125**, 1–15.

Fitzpatrick, J. W. (1980). Foraging behavior of neotropical tyrant flycatchers. *Condor* **82**, 43–57.

Hedenström, a, Rosén, M. and Spedding, G. R. (2006). Vortex wakes generated by robins Erithacus rubecula during free flight in a wind tunnel. *J. R. Soc. Interface* **3**, 263–276.

Heers, A. M., Tobalske, B. W. and Dial, K. P. (2011). Ontogeny of lift and drag production in ground birds. *J. Exp. Biol.* **214**, 717–725.

Henningsson, P., Hedenström, A. and Bomphrey, R. J. (2014). Efficiency of lift production in flapping and gliding flight of swifts. *PLoS One* **9**,.

Jackson, B. E. and Dial, K. P. (2011). Scaling of mechanical power output during burst escape flight in the Corvidae. *J. Exp. Biol.* **214**, 452–461.

Jetz, W., Thomas, G. H., Joy, J. B., Hartmann, K. and Mooers, A. O. (2012). The global diversity of birds in space and time. *Nature* **491**, 444–448.

Lentink, D., Müller, U. K., Stamhuis, E. J., de Kat, R., van Gestel, W., Veldhuis, L. L. M., Henningsson, P., Hedenström, A., Videler, J. J. and van Leeuwen, J. L. (2007). How swifts control their glide performance with morphing wings. *Nature* **446**, 1082–1085.

Pennycuick, C. J. (1968). A wind-tunnel study of gliding flight in the pigeon *Columba livia*. *J. Exp. Biol.* **49**, 509–526.

Polhamus, E. C. (1966). A concept of the Vortex Lift of Sharp-Edge Delta Wings Based on a Leading-Edge-Suction Analogy. *Natl. Aeronaut. Sp. Adm.* **Nasa Techn**,.

Provini, P., Tobalske, B. W., Crandell, K. E. and Abourachid, A. (2012). Transition from leg to wing forces during take-off in birds. *J. Exp. Biol.* 4115–4124.

Provini, P., Tobalske, B. W., Crandell, K. E. and Abourachid, A. (2014). Transition from wing to leg forces during landing in birds. *J. Exp. Biol.* 2659–2666.

R Core Team (2015). R: A language and environment for statistical computing.

Rayner, J. V. (1988). Form and Function in Avian Flight. In *Current Ornithology SE - 1* (ed. Johnston, R.), pp. 1–66. Springer US.

Rayner, J. M. V. (1999). Estimating power curves of flying vertebrates. *J. Exp. Biol.* **202**, 3449–3461.

Revell, L. J. (2012). phytools: an R package for phylogenetic comparative biology (and other things). *Methods Ecol. Evol.* **3**, 217–223.

Reynolds, K. V., Thomas, A. L. R. and Taylor, G. K. (2014). Wing tucks are a response to atmospheric turbulence in the soaring flight of the steppe eagle *Aquila nipalensis*. *J. R. Soc. Interface* **11**, 20140645.

Savile, D. B. O. (1957). Adaptive evolution in the avian wing. *Evolution (N. Y).* **11**, 212–224.

Schneider, C. A., Rasband, W. S. and Eliceiri, K. W. (2012). NIH Image to ImageJ: 25 years of image analysis. *Nat. Methods* **9**, 671–675.

Shaffer, S. A., Costa, D. P. and Weimerskirch, H. (2001). Behavioural factors affecting foraging effort of brreeding wandering albatrosses. *J. Anim. Ecol.* **70**, 864–874.

Spedding, G. R. and McArthur, J. (2010). Span Efficiencies of Wings at Low Reynolds Numbers. *J. Aircr.* **47**, 120–128.

Spedding, G. R., Rosén, M. and Hedenström, a (2003). A family of vortex wakes generated by a thrush nightingale in free flight in a wind tunnel over its entire natural range of flight speeds. *J. Exp. Biol.* **206**, 2313–2344.

The Mathworks Inc. MATLAB and Statistics Toolbox Release.

Tobalske, B. W. (1996). Scaling of muscle composition, wing morphology, and intermittent flight behavior in woodpeckers. *Auk* **113**, 151–177.

Tobalske, B. W. (2001). Morphology, Velocity, and Intermittent Flight in Birds. *Am. Zool.* **41**, 177–187.

Tobalske, B. W. (2007). Biomechanics of bird flight. *J. Exp. Biol.* **210**, 3135–3146.

Tobalske, B. W. and Dial, K. P. (1996). Flight kinematics of black-billed magpies and pigeons over a wide range of speeds. *J. Exp. Biol.* **199**, 263–80.

Tobalske, B. W. and Dial, K. P. (2000). Effects of body size on take-off flight performance in the Phasianidae (Aves). *J. Exp. Biol.* **203**, 3319–3332.

Tobalske, B. W., Hedrick, T. L. and Biewener, A. A. (2003a). Wing kinematics of avian flight across speeds. *J. Avian Biol.* **34**, 177–184.

Tobalske, B. W., Hedrick, T. L., Dial, K. P. and Biewener, A. A. (2003b). Comparative power curves in bird flight. *Nature* **421**, 363–6.

Tobalske, B. W., Puccinelli, L. A. and Sheridan, D. C. (2005). Contractile activity of the pectoralis in the zebra finch according to mode and velocity of flap-bounding flight. *J. Exp. Biol.* **208**, 2895–2901.

Tucker, V. A. (1987). Gliding birds: the effect of variable wing span. *J. Exp. Biol.* **133**, 33–58.

Tucker, V. A. (1993). Gliding birds: reduction of induced drag by wing tip slots between the primary feathers. *J. Exp. Biol.* **180**, 285–310.

Tucker, V. A. (1995). Drag reduction by wing tip slots in a gliding Harris' hawk, *Parabuteo unicinctus* . *J. Exp. Biol.* **198**, 775–81.

Tucker, V. A. and Parrott, G. C. (1970). Aerodynamics of gliding flight in a falcon and other birds. *J. Exp. Biol.* **52**, 345–367.

Usherwood, J. R. (2009). The aerodynamic forces and pressure distribution of a revolving pigeon wing. *Exp. Fluids* **46**, 991–1003.

Usherwood, J. R. and Ellington, C. P. (2002a). The aerodynamics of revolving wings I. Model hawkmoth wings. *J. Exp. Biol.* **205**, 1547–1564.

Usherwood, J. R. and Ellington, C. P. (2002b). The aerodynamics of revolving wings II. Propeller force coefficients from mayfly to quail. *J. Exp. Biol.* **205**, 1565–1576.

van den Hout, P. J., Mathot, K. J., Maas, L. R. M. and Piersma, T. (2010). Predator escape tactics in birds: Linking ecology and aerodynamics. *Behav. Ecol.* **21**, 16–25.

Viieru, D., Tang, J., Lian, Y., Liu, H. and Shyy, W. (2006). Flapping and Flexible Wing Aerodynamics of Low Reynolds Number Flight Vehicles. *44th AIAA Aerosp. Sci. Meet. Exhib.* 1–18.

Vogel, S. (1996). *Life in moving fluids: The physical biology of flow*. 2nd ed. Princeton, NJ: Princeton University Press.

Wang, Z. J., Birch, J. M. and Dickinson, M. H. (2004). Unsteady forces and flows in low Reynolds number hovering flight: two-dimensional computations vs robotic wing experiments. *J. Exp. Biol.* **207**, 449–460.

Weimerskirch, H., Guionnet, T., Martin, J., Shaffer, S. a and Costa, D. P. (2000). Fast and fuel efficient? Optimal use of wind by flying albatrosses. *Proc. Biol. Sci.* **267**, 1869–1874.

Withers, P. C. (1981). An aerodynamic analysis of bird wings as fixed aerofoils. *J. Exp. Biol.* **90**, 143–162.

Table 1: Morphological and experimental attributes of specimen wings.

	Species	Common Name	4-Letter Abbr.	Mass (g)	Angular Vel. (rad/sec)	Area (m^2)		Length (m)		Aspect Ratio		Sweep Angle		Feather Emargination		Reynolds Number	
						Ext	Swept	Ext	Swept	Ext	Swept	Ext	Swept	Ext	Swept	Ext	Swept
Falconidae	Falco sparverius	American kestrel	AMKE	80.8	46.7	0.017	0.011	0.285	0.201	4.7	3.6	176	109	8.08	2.24	370,000	400,000
	Falco columbarius	Merlin	MERL	146.9	40.9	0.031	0.015	0.338	0.158	3.7	1.7	159	78	1.69	0.13	570,000	600,000
	Falco peregrinus	Peregrine falcon	PEFA	762.8	31.9	0.051	0.036	0.487	0.326	4.7	3	131	92	0.47	0.22	770,000	810,000
Accipitridae	Accipiter striatus	Sharp-shinned hawk	SSHA	161.1	40.2	0.019	0.015	0.308	0.219	5	3.1	157	113	2.52	1.56	450,000	450,000
	Circus cyaneus	Northern harrier	NOHA	420*	32.6	0.053	0.037	0.443	0.283	3.7	2.2	136	88	3.75	0.7	800,000	850,000
	Accipiter gentilis	Northern goshawk	NOGO	420*	32.6	0.065	0.054	0.459	0.366	3.2	2.5	147	112	1.79	0.81	960,000	920,000
	Accipiter cooperii	Cooper's hawk	COHA	452.2	32	0.049	0.039	0.432	0.337	3.8	2.9	159	120	3.95	1.56	750,000	780,000
	Buteo lagopus	Rough-legged hawk	RLHA	820	19.6	0.097	0.076	0.635	0.423	4.1	2.4	169	113	2.8	0.33	890,000	1,060,000
	Buteo jamaicensis	Red-tailed hawk	RTHA	1250*	17.2	0.100	0.075	0.666	0.526	4.5	3.7	178	119	3.19	1.19	880,000	1,130,000
Strigidae	Aegolius acadicus	Northern saw-whet owl	NSWO	92.6	45.3	0.013	0.011	0.220	0.170	3.6	2.7	138	104	0.64	0.45	430,000	420,000
	Megascops kennicottii	Western screech-owl	WESO	214.3	37.8	0.026	0.017	0.315	0.203	3.7	2.5	163	101	4.9	0.74	580,000	590,000
	Asio otus	Long-eared owl	LEOW	258.2	36.2	0.046	0.034	0.427	0.322	4	3	147	104	2.82	0.93	680,000	700,000
	Bubo virginianus	Great Horned owl	GHOW	1860	15.2	0.127	0.115	0.670	0.573	3.5	2.9	189	142	1.7	0.3	1,030,000	1,290,000

* masses are estimates from Dunning Jr. (1992).

Table 2: Summary of results of statistical tests (p-values) for significant effects of posture, flight style, and morphology upon aerodynamic performance of wings of 13 species of raptors (phylogenetic ANOVA for all; * indicates p<0.05).

	Extended AR	Emargination	Log(extended area)	Wing loading	Log(mass)
Extended Gliding	0.87	0.69	.005*	0.25	0.02*
Swept Gliding	0.53	0.64	0.061	0.17	0.06
Extended Flapping	0.48	0.59	0.07	0.87	0.19
Swept Flapping	1.00	0.94	.036*	0.69	0.14

Table 3: Peak coefficients of vertical and horizontal force, C_V and C_H, observed during experiments using wings from 13 species of raptors.

	Species	Extended Gliding		Swept Gliding		Gliding C_V:C_H		Extended Flapping		Swept Flapping		Flapping C_V:C_H	
		Peak C_V	Peak C_H	Peak C_V	Peak C_H	Extended	Swept	Peak C_V	Peak C_H	Peak C_V	Peak C_H	Extended	Swept
Falconidae	Falco sparverius	0.88	0.9	1.01	0.87	3.15	3.48	1.2	0.96	0.93	1	3.69	2.64
	Falco columbarius	0.82	0.76	1.08	0.84	3.19	2.8	1.22	0.91	0.94	0.82	2.9	1.41
	Falco peregrinus	1.14	0.94	1.39	0.81	4.95	3.59	1.47	0.91	0.8	0.66	3.6	1.45
Accipitridae	Accipiter striatus	0.95	0.89	1.11	0.78	4.29	6.45	1	0.82	1.1	1.06	3.1	2.26
	Circus cyaneus	0.94	0.69	1.34	0.78	4.96	3.41	1.2	0.66	1.12	0.69	4.56	3.47
	Accipiter gentilis	1.18	0.95	1.16	0.88	6.3	5.09	1.53	0.96	0.87	0.64	4.54	3.23
	Accipiter cooperii	0.94	0.81	1.03	0.8	5.24	4.17	1.21	0.66	0.99	0.71	4.7	2.91
	Buteo lagopus	1.31	0.9	0.94	0.67	5.98	5.94	1.95	1.25	1	0.68	4.75	2.89
	Buteo jamaicensis	1.21	0.98	1.06	0.77	6.24	6.42	1.76	1.45	1.24	1.07	3.49	2.76
Strigidae	Aegolius acadicus	1	0.71	1.01	0.77	3.52	3.24	1.77	1.51	0.9	1.26	2.1	1.47
	Megascops kennicottii	0.84	0.78	1.3	0.83	3.3	3.04	1.47	1.09	0.68	0.5	3.1	1.37
	Asio otus	0.95	0.52	1.06	0.66	5.62	5.33	0.67	0.23	1.14	0.66	3.93	3.17
	Bubo virginianus	1.36	0.82	1.02	0.68	4.95	7.9	1.86	1.29	1.12	0.71	3.68	4.25
	Average	1.04	0.82	1.12	0.78	4.75	4.68	1.41	0.98	0.99	0.80	3.70	2.56
	SD (±)	0.17	0.12	0.14	0.07	1.11	1.56	0.36	0.34	0.15	0.21	0.76	0.88

Figures

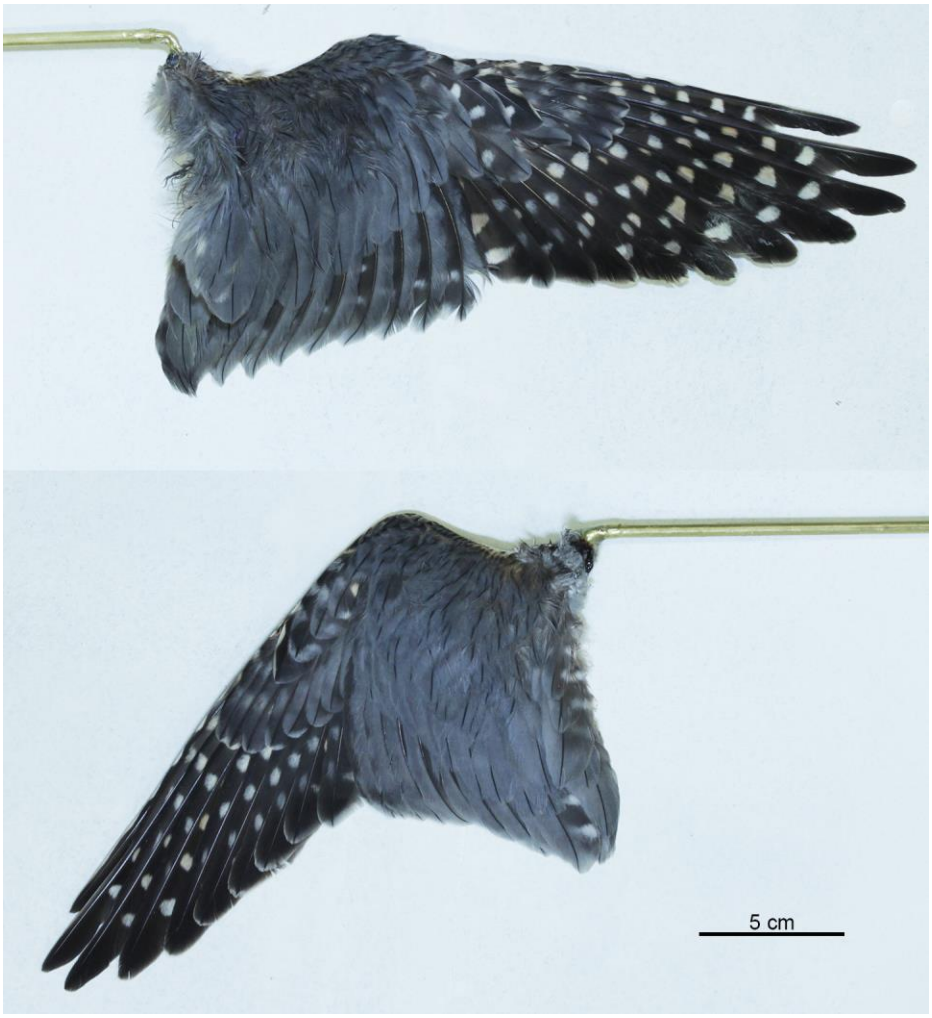

Figure 1: Swept and Extended wings – Birds are capable of morphing their wings into a swept and extended configuration, resulting in reduced area, increased leading edge angle, and reduction of wing-tip slots. Pictured here are the wings of a sharp-shinned hawk (*Accipiter striatus*).

Journal of Experimental Biology • Advance article

(a)

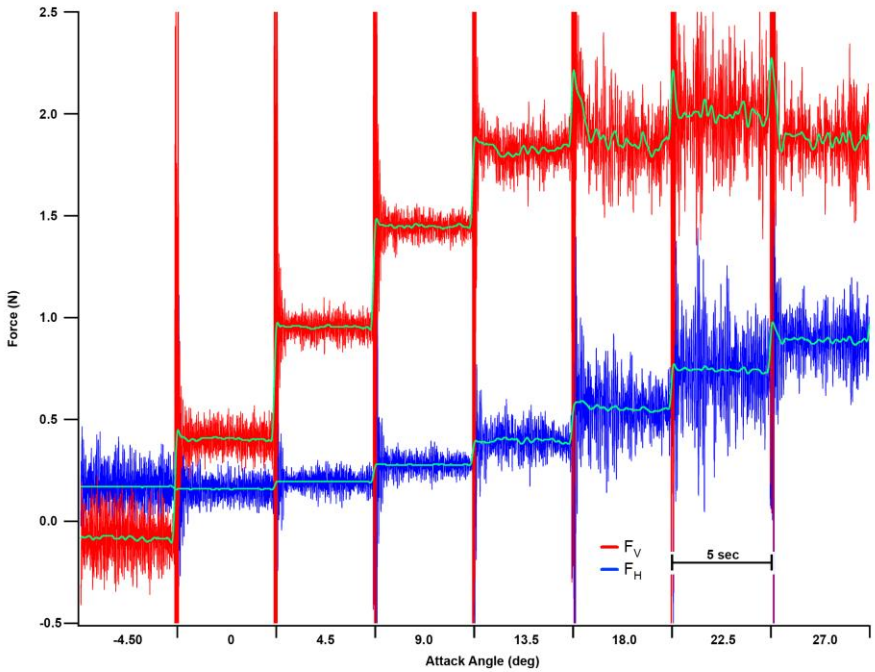

(b)

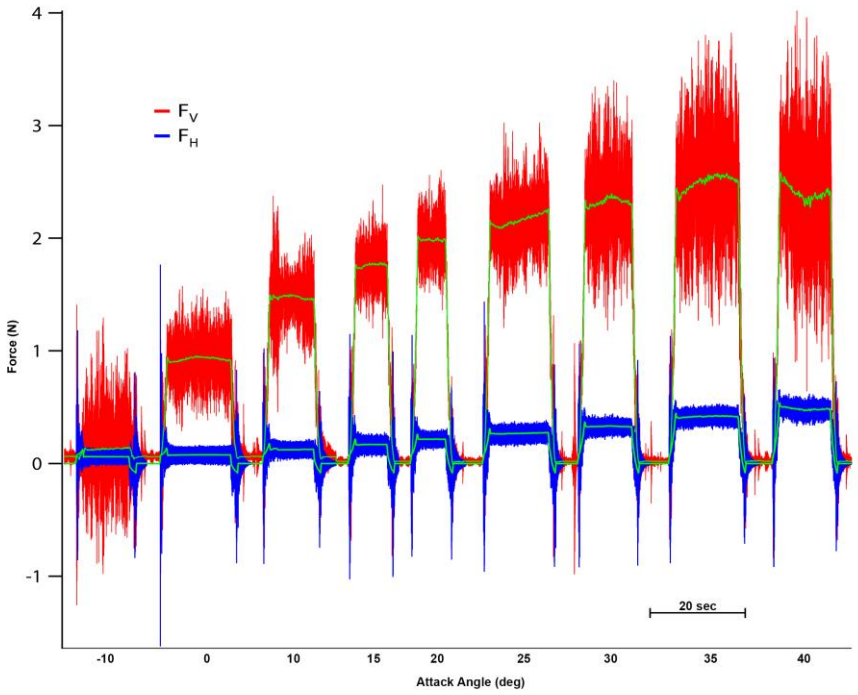

Figure 2: Actual force measures for peregrine falcon (*Falco peregrinus*) extended wing in gliding flight (a) and flapping flight (b). Sample taken at 1000 Hz. Green lines represent data filtered at 3 Hz using a low-pass Butterworth filter.

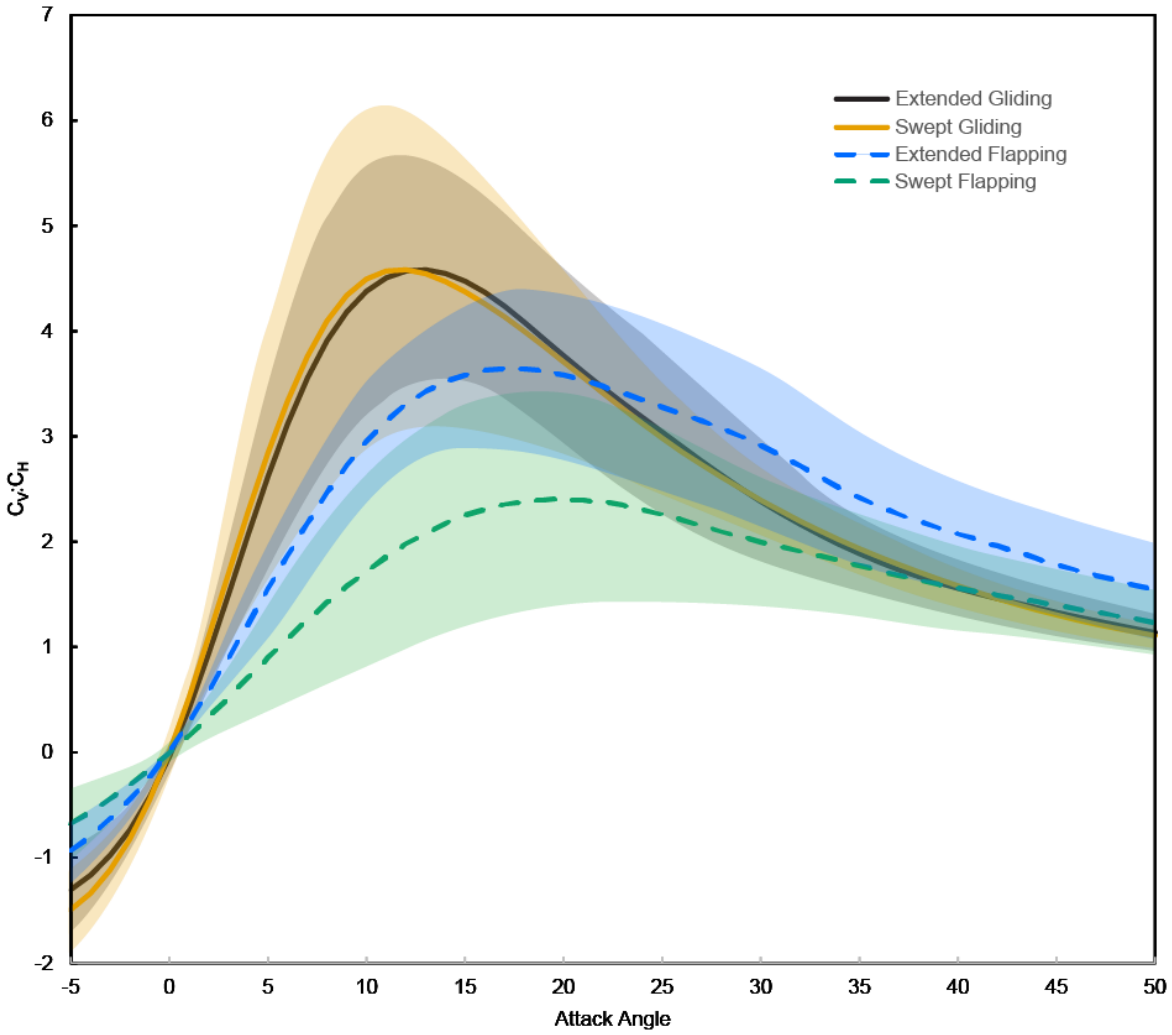

Figure 3: Average ratios of vertical to horizontal force coefficient (C_V:C_H) as a function of angle of attack (α) of the wing for all species (N=13). The shaded regions represent ± SD.

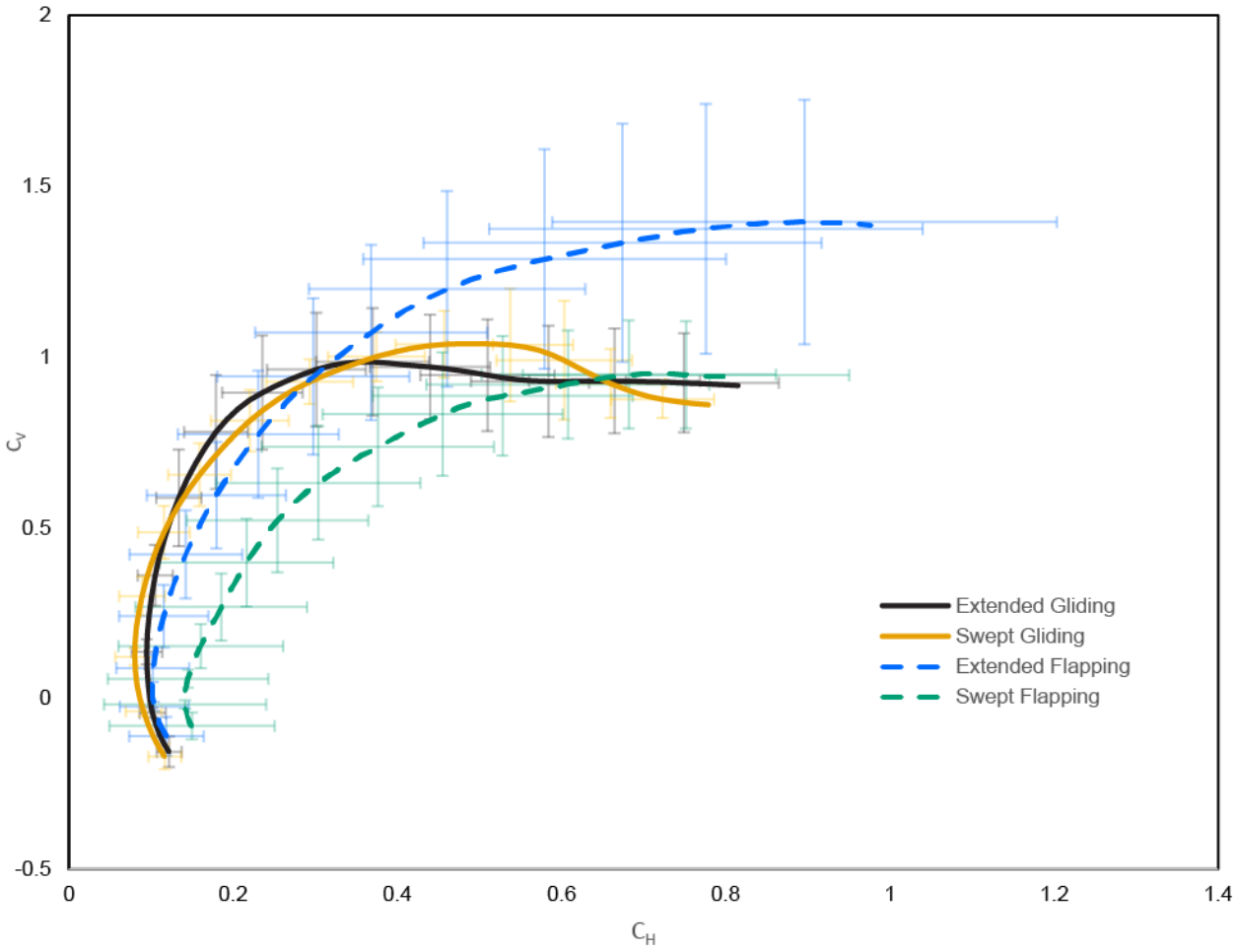

Figure 4: Mean vertical force coefficient (C_V) as a function of mean horizontal force coefficient (C_H) for wings of 13 raptor species. Error bars indicate ± SD for C_V and C_H.

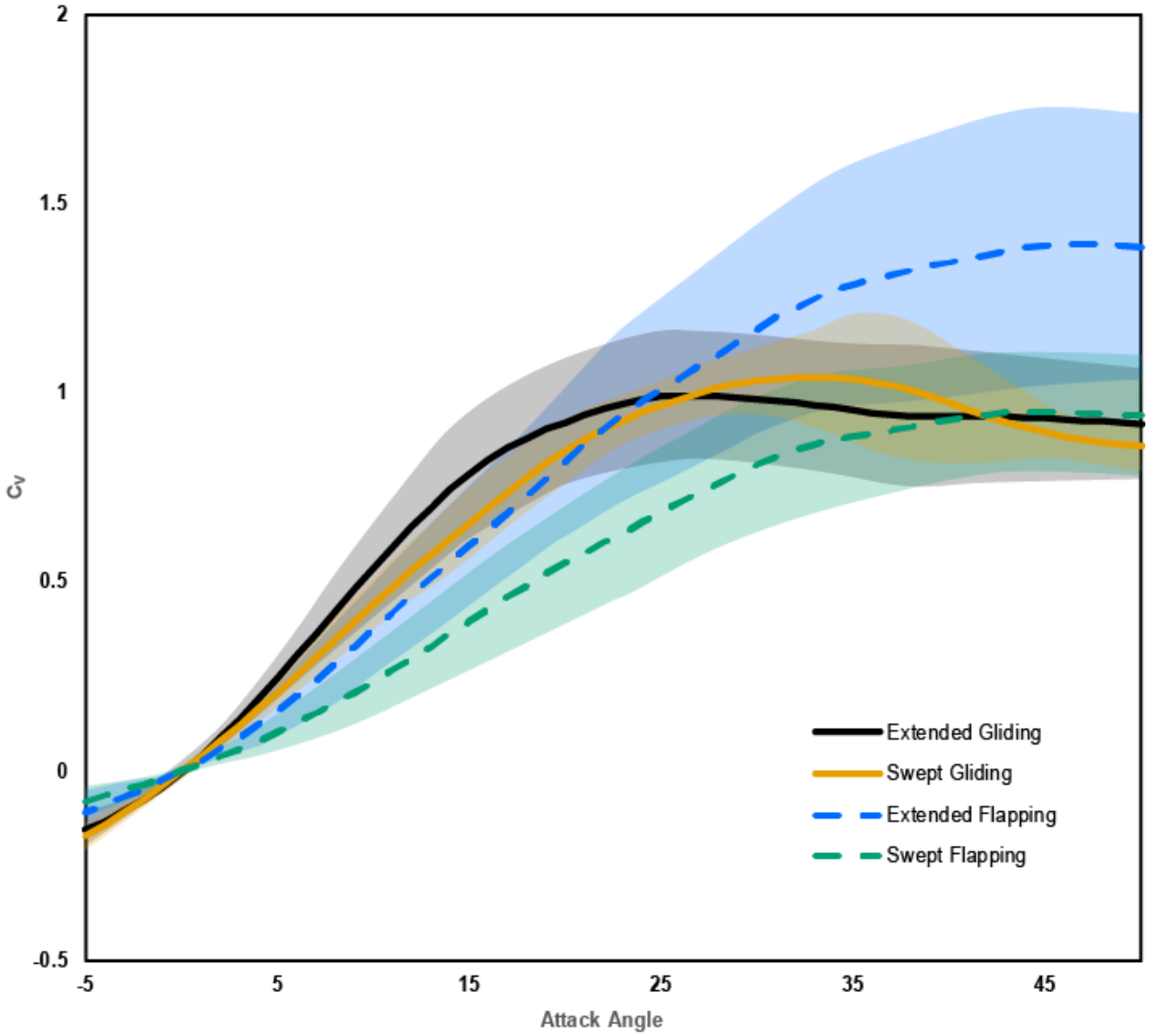

Figure 5 : C_V as a function of attack angle in extended and swept postures during emulated flapping and gliding. The shaded regions represent ± SD.

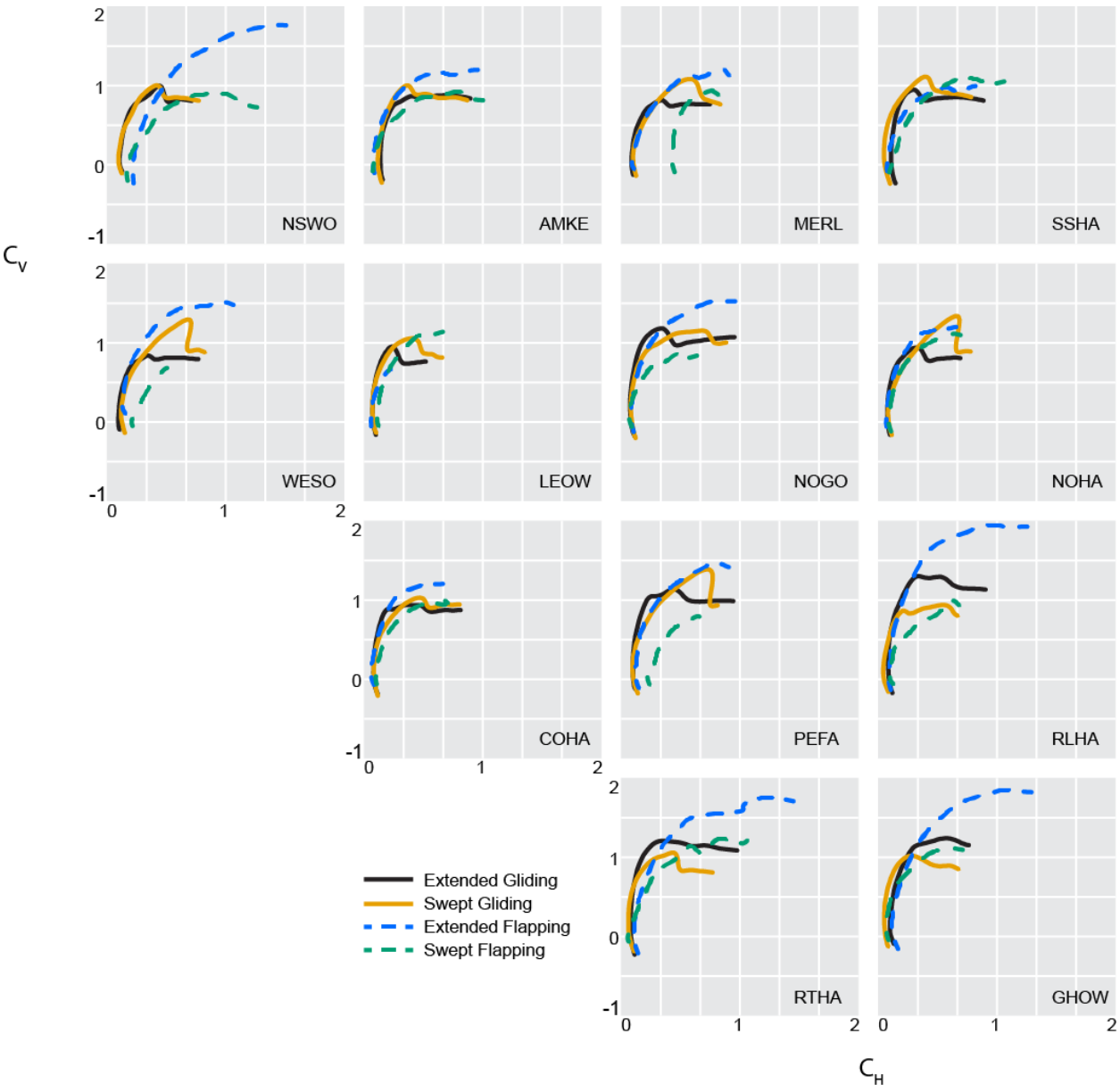

Figure 6: Individual polars of C_V as a function of C_H for wings of 13 raptor species configured in extended and swept postures and either spun as a propeller to emulate flapping flight or mounted in a wind tunnel to emulate gliding flight.

Table S1

Click here to Download Table S1

Table S2

Click here to Download Table S2